Bursting dynamics in a spiking neuron with a memristive voltage-gated channel

Jiaming Wu, Kang Wang, Olivier Schneegans, Pablo Stoliar, Marcelo Rozenberg

▶ **To cite this version:**

Jiaming Wu, Kang Wang, Olivier Schneegans, Pablo Stoliar, Marcelo Rozenberg. Bursting dynamics in a spiking neuron with a memristive voltage-gated channel. Neuromorphic Computing and Engineering, 2023, 3 (4), pp.044008. 10.1088/2634-4386/ad139b . hal-04495719

HAL Id: hal-04495719
https://hal.science/hal-04495719v1

Submitted on 10 Oct 2024

HAL is a multi-disciplinary open access archive for the deposit and dissemination of scientific research documents, whether they are published or not. The documents may come from teaching and research institutions in France or abroad, or from public or private research centers.

L'archive ouverte pluridisciplinaire **HAL**, est destinée au dépôt et à la diffusion de documents scientifiques de niveau recherche, publiés ou non, émanant des établissements d'enseignement et de recherche français ou étrangers, des laboratoires publics ou privés.

Distributed under a Creative Commons Attribution 4.0 International License

Neuromorphic Computing and Engineering

PURPOSE-LED PUBLISHING™

PAPER • **OPEN ACCESS**

Bursting dynamics in a spiking neuron with a memristive voltage-gated channel

To cite this article: Jiaming Wu *et al* 2023 *Neuromorph. Comput. Eng.* **3** 044008

View the article online for updates and enhancements.

You may also like

- Brain-inspired nanophotonic spike computing: challenges and prospects
Bruno Romeira, Ricardo Adão, Jana B Nieder et al.
- Exploiting deep learning accelerators for neuromorphic workloads
Pao-Sheng Vincent Sun, Alexander Titterton, Anjlee Gopiani et al.
- Optical spike amplitude weighting and neuromimetic rate coding using a joint VCSEL-MRR neuromorphic photonic system
Matj Hejda, Eli A Doris, Simon Bilodeau et al.

This content was downloaded from IP address 89.159.53.40 on 10/10/2024 at 15:54

IOP Publishing Neuromorph. Comput. Eng. 3 (2023) 044008 https://doi.org/10.1088/2634-4386/ad139b

NEUROMORPHIC
Computing and Engineering

CrossMark

OPEN ACCESS

RECEIVED
10 July 2023

ACCEPTED FOR PUBLICATION
8 December 2023

PUBLISHED
29 December 2023

Original Content from this work may be used under the terms of the Creative Commons Attribution 4.0 licence.

Any further distribution of this work must maintain attribution to the author(s) and the title of the work, journal citation and DOI.

PAPER

Bursting dynamics in a spiking neuron with a memristive voltage-gated channel

Jiaming Wu[1], **Kang Wang**[1], **Olivier Schneegans**[2], **Pablo Stoliar**[3] **and Marcelo Rozenberg**[1,*]

[1] Université Paris-Saclay, CNRS Laboratoire de Physique des Solides, 91405 Orsay, France
[2] Laboratoire Génie électrique et électronique de Paris, CentraleSupélec, CNRS, Sorbonne Université and Université Paris-Saclay, 91192 Gif-sur-Yvette, France
[3] National Institute of Advanced Industrial Science and Technology (AIST), 305-8565 Tsukuba, Japan
[*] Author to whom any correspondence should be addressed.

E-mail: marcelo.rozenberg@universite-paris-saclay.fr

Keywords: memristor, spiking neuron, bursting

Abstract

We introduce a voltage-gated conductance model for an artificial neuron that exhibits tonic, fast, and two types of intrinsic burst spiking. The spike generation is achieved with a single voltage-gated channel that exploits the conductance commutation properties of a two-terminal memristive device. Our circuit implementation is of unprecedented simplicity, using just four electronic components, all conventional, cheap and out-of-the-shelf. Our bursting neuron is a two-compartment model, similar to the Pinsky–Rinzel model. We obtain the full phase diagram and discuss the origin of the different regions. We find that the spike traces of the model bare striking similarity to experimental biological neuronal recordings. Our work may open a new way to investigate neural pathologies, such as epilepsy and Parkinson's disease, from the study of the phase diagram and the transitions between spiking states of physical neuron models.

1. Introduction

The understanding of neural networks is one of the current great scientific challenges. The interest in this problem spans a wide range of fields. From applications in artificial intelligence, such as robotics and marketing, to neuroscience, such as elucidating the mechanism of cognitive functions in animal and human brains.

The variety of methodological approaches to tackle the problem is equally vast and multidisciplinary. At the core of neural networks are neuron models [1, 2] whose great variety also reflect the diversity of the field. They range from abstract mathematical models, such as the two-state neurons in the Hopfield's model [3], to sets of coupled differential equations in biologically realistic Hodgkin–Huxley models [4], to digital electronic implementations in neuromorphic chips [5, 6], or even to quantum materials with exotic metal–insulator transition behavior such as the Mott insulators [7–10].

Here we shall focus on a novel spiking neuron model, which is at the crossroad of those approaches. An important point to make is that the present neuron model *is defined by its hardware implementation*. While a mathematical model is defined by a set of equations, here our model is defined by a *circuit*. Significantly, our circuit-model emulates the simplicity of the simplest mathematical models, such as the integrate-and-fire (IF) or Izhikevich's [2, 11, 12]. It also shares the basic structure of all biological neuron models, where the cell membrane is represented by a capacitor whose charge is affected by the behavior of ionic conductance channels [2, 4, 12]. The nonlinear conductance in our neuron model is realized by a *memristive* device, [13–16] which allows to resolve the apparent contradiction of complex dynamical behavior with circuit simplicity. A memristor is a two-terminal resistive component whose value of resistance can change depending on the applied voltage and has hysteresis, i.e. a memory effect. A simple and practical definition of

© 2023 The Author(s). Published by IOP Publishing Ltd

a memristor device was provided by Chua [14]: it is a device that exhibits a 'pinched' hysteresis loop (*see* top left panel of figure 2).

The relevance of memristive materials for neuromorphic engineering applications has been recently acknowledged and is developing fast [17–19]. There are various proposals for the implementation of spiking neurons based on memristive materials. Almost all of them adopt Mott insulators, which are quantum materials that exhibit insulator-to-metal transitions. For instance, the 'neuristor' [8] based on the the Mott compound NbO_2, which is an approximate realization of the Hodgkin–Huxley neuron model. With a similar neuristor model, based on the Mott compound VO_2, it was demonstrated that it could capture as many as 23 different biological spiking behaviors [9]. Another type of Mott materials, the $GaTa_4Se_8$ compound that showed a resistive collapse upon the application of a train of voltage spikes [20], was adopted to implement the basic leaky-IF (LIF) neuron model [7]. While Mott materials show a great promise to implement low-power neuromorphic hardware, they also face significant challenges [15, 16, 18]. Their complex fabrication methods require improvements to achieve a reproducible sample-to-sample behavior, long-term reliability and to function at room temperature. On the theory side, the description of the behavior of Mott insulators out-of-equilibrium is an open problem, and the physical mechanisms of the resistive collapse are being explored and debated [10, 21]. Those are the main reasons why the current research on spiking neuron models using Mott materials is still at the level of the single device characterization. The integration of Mott neurons into *functional neural networks*, beyond numerical simulations, remains an open challenge.

In the present work, we exploit the simplicity of the *memristor concept* for a spiking neuron model, while avoiding the practical issues described above. We adopt a new type of memristor device, which is obtained by the combination of two *conventional* electronic components, a resistor and a thyristor. A key insight is to realize that this memristive device has the same qualitative I–V characteristic as it is observed in the Mott quantum materials discussed above [8].

A main result of the present work is to introduce a voltage-gated conductance model of unprecedented simplicity, which realizes four basic behaviors relevant to biological neurons: tonic, fast and two types of intrinsic burst spiking. In what follows, we first provide a pedagogical description of the implementation of an IF artificial neuron model with our memristive device. We try to keep the discussion close to the concepts used in Neuroscience, so as to build a bridge between the different disciplines. Then, we build on that basic model, adding a second compartment that introduces a new timescale, to obtain complex burst-spiking behavior. Quite remarkably, we find that the voltage traces of our circuit model bare a striking resemblance to biological ones measured in rats, including their typical time scales. We then further exploit the simplicity of our neuron model to obtain the full phase diagram, with four regions that correspond to four different spiking states. This phase diagram reveals the global behavior of the two-compartment model and leads to a speculative but also exciting observation. Namely, that the systematic changes experimentally induced in rats' bursting neurons, seem to follow paths on the phase diagram of our bursting neuron model.

2. The memristive spiking neuron model

In basic IF spiking neuron models the *integrate* function is always assured by a capacitor C_m that represents the membrane of the neuron. Its charge is the integral of the input current I_{in} to the neuron, which results in the membrane potential $V = Q/C_m = \int I_{in} dt/C_m$. On the other hand, the *fire* function is an electric spike, due to the closing of a switch and the sudden discharge of the capacitor, when the potential attains a threshold value V_{th} (see figures 1(a)–(c)).

In more realistic, conductance-based mathematical models [2, 12], the spike generation mechanism is achieved by voltage-gated channels (figure 1(c) shows a single channel for simplicity), which respond non-linearly to the applied voltage and control the charge and discharge of the C_m. Those models share a similar mathematical structure and are defined by a set of equations of the form,

$$C_m \frac{dV}{dt} = I_{ion}(t) + I_{in}(t) = \Sigma_k I_k(t) + I_{in}(t) \quad (1)$$

$$I_k(t) = g_k(V, S_k)\, V \quad (2)$$

where I_k are the channel currents and $g_k(V, S_k)$ are the respective voltage-gated conductances. The variable S_k indicates the 'state' of the conductance and it may also depend on time. Two notable examples are the Hodgkin–Huxley model and its simplified version, the Morris–Lecar model [2, 12]. The conductance channels g_k are defined by dynamical equations that characterize the dependence of the conductance with the voltage and other internal states of the channel. In order to generate an action potential spike, the multiple

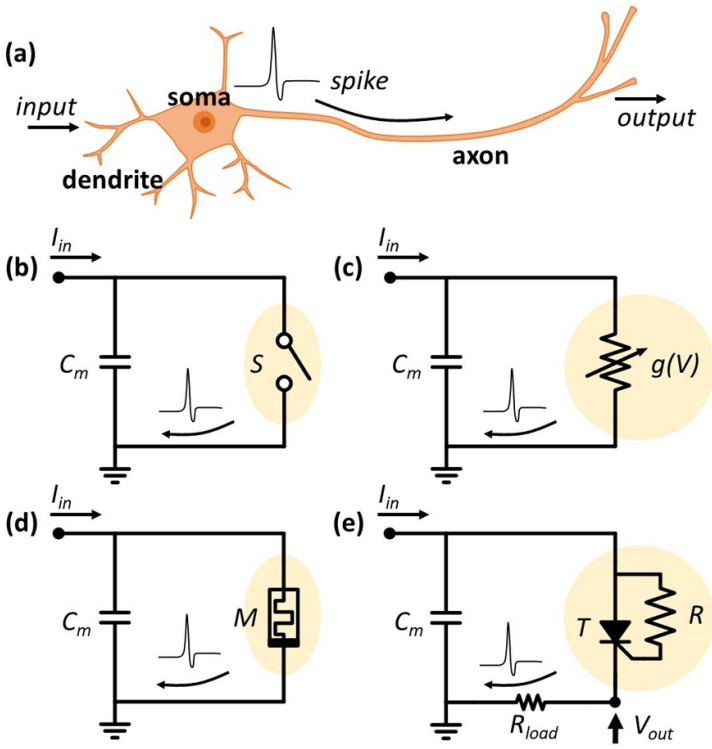

Figure 1. (a) Schematic of a biological neuron. (b) Basic integrate-and-fire model. (c) Schematic of nonlinear conductance channel model. (d) Integrate-and-fire model using a memristor; (e) MSN model circuit showing the two-terminal memristor obtained from the combination of a thyristor and a resistor. In the circuit we add a small load resistor $R_{\rm load}$ after the M device to measure the spike traces by the voltage $V_{\rm out}$.

channels need to successively open and close [2, 12]. For instance, in the basic form of the Hodgkin–Huxley model the gated channels are two, one for sodium and one for potassium. However, adopting a memristive channel we can reduce the number of channels to just one. The formal mathematical definition of the memristor is rather involved and beyond the scope of the present work. Here, we shall simply call a memristor a two terminal device, whose current value of resistance depends on its applied voltage and shows hysteresis. In the interest to remain closest to the concepts of neuroscience models, we shall consider here the conductance of the memristor, i.e. the inverse of its resistance.

The memristive spiking neuron (MSN) model shown in figure 1(d) shares the same form as the models mentioned above. However, as will become clear later on, the spike generation in the MSN does not require of multiple voltage-gated channels but just a single one. Key to this feature is that the channel's conductance is history-dependent or *memristive*. To describe the spike generation in this model we focus on its simplest version, with a single memristive channel, that implements a (leaky) IF model. As shown in figure 1(d), the voltage-threshold switch of the IF model is implemented by the memristive conductance M. As will become clear below, depending on the applied voltage and its past history, this two-terminal device commutes from open (low conductance $g_{\rm low}$) to closed (high conductance $g_{\rm high}$) states and back. Initially, the memristor is in the open state allowing the membrane capacitor to increase its charge by integrating the applied input current. When its potential reaches a given $V_{\rm th}$ the memristor commutes to the closed state and the capacitor discharges emitting a spike of current. At the end of the discharge, when a low reset membrane voltage $V_{\rm res} < V_{\rm th}$ is reached, the memristor commutes back to the open state and the charging of the membrane starts anew. Therefore, this memristive circuit realizes the basic tonic spiking mechanism of an IF model under a constant current injection.

We now show how these qualitative considerations can be practically implemented with a memristive conductance using conventional electronic components. We simply connect a resistor (R) between the anode and gate electrodes of a thyristor (T), to obtain the two-terminal M device, as shown in figure 1(e).

The thyristor is a conventional electronic component, introduced in the 50s [22]. Its behavior can be most simply described as that of a diode with a threshold. A diode is a *pn*-junction that conducts current for

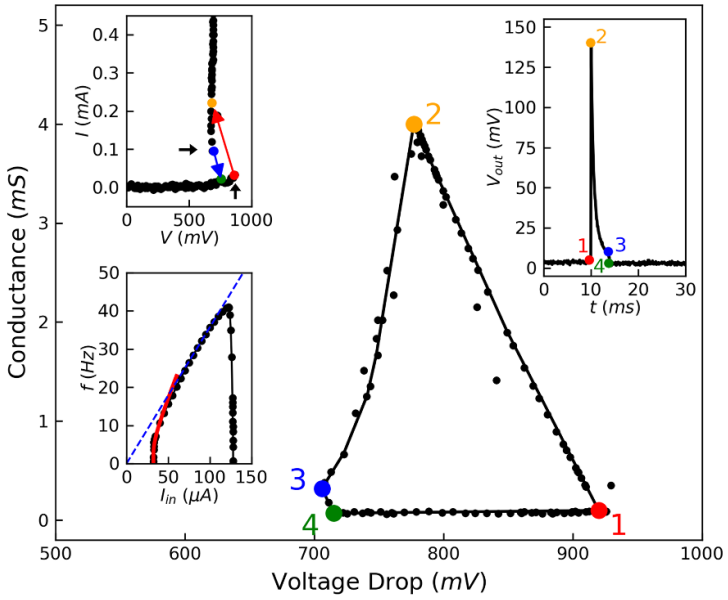

Figure 2. Spiking behavior of the MSN-IF model of figure 1(e) for $R = 100\,\mathrm{k}\Omega$ and $C_\mathrm{m} = 10\mu\mathrm{F}$, which are kept fixed for the whole present work if not specifically indicated. (Main panel) The conductance commutation of the memristive voltage-gated channel $g(V)$ during the cycle of spike generation. The x-axis corresponds to the voltage between the two terminals of M, and the y-axis to its two-terminal conductance. The commutation is correlated by the color dots with the spike trace (right panel). The I–V characteristic of the M device (top left panel) was obtained using the circuit shown in methods section figure 7(a). The color dots of the I–V indicate the work-points associated to the instants along the trace and along the orbit. The small black arrows in the I–V indicate the holding current I_hold ($\approx$0.1 mA) and the threshold voltage V_th ($\approx$0.9 mV). (Bottom left panel) The spiking frequency as a function of applied current $f(I_\mathrm{in})$. The dotted line (blue) indicates the linear ideal IF behavior. The solid line (red) is a fit using the LIF-model type 1 excitability form $f(I_\mathrm{in}) \propto -1/\log(1 - I_\mathrm{in}^\mathrm{min}/I_\mathrm{in})$ [2]. The neuron is excited in a finite range of input currents $I_\mathrm{in}^\mathrm{min} < I_\mathrm{in} < I_\mathrm{in}^\mathrm{max}$, with $I_\mathrm{in}^\mathrm{min} = 32.3\,\mu$A and $I_\mathrm{in}^\mathrm{max} = 127.9\,\mu$A. Main and right panel data were measured at $I_\mathrm{in} = 92.4\,\mu$A with small $R_\mathrm{load} = 47\,\Omega$; top left panel data were measured with the M in series with a 1 kΩ resistor; bottom left panel data were measured with a small $R_\mathrm{load} = 47\,\Omega$.

one (direct) polarity and has negligible conductance for the opposite (inverse) one. A thyristor is a *pnpn*-device, so in direct has two *pn* junctions that conduct but has one *np* that is inverted, which creates a *depletion region* and does not conduct. However, by injecting electrons through the thyristor gate the depletion layer gets 'flooded' and the device suddenly starts to conduct between its anode and cathode.

In our two-terminal memristor device this commutation is simply achieved by the R connected between the anode and gate of the T (figure 1(e)) by the following mechanism: when the T is non-conducting the depletion layer is in place. Then, a small current finds a smaller resistance path, flowing through the R and into the gate electrode. As the applied voltage increases, the small current increases and electrons entering the gate electrode start to populate ('flooding') the depletion layer. When the applied voltage (or the gate current) reaches a certain threshold, the depletion layer suddenly collapses and the two-terminal anode–cathode conductance commutes. Importantly, this high conductive state remains self-sustained by the relatively high current density flowing, until it falls beneath a small 'holding' current value I_hold (equivalent to the V_res see above), where the depletion region forms again. At that point the two-terminal memristor device commutes back to low conductance state.

From this description, one can readily understand the hysteretic behavior of the 'pinched' I–V loop of the two-terminal M device, shown in the top left inset panel of figure 2. As the anode–cathode voltage V is increased, the gate current injected through R also increases. When this current becomes significant, the resistance of the T, hence of the M, suddenly collapses and the current I surges vertically (red-dot to yellow-dot). By decreasing the applied V the hysteresis becomes apparent, until the I decreases beneath the holding value and the high resistance state is recovered (blue-dot to green-dot). It is a key insight to realize that the I–V characteristics of the present memristive device are qualitatively identical to the Mott memristors, as, for instance, in the implementation of the 'neuristor' [8]. One word of warning is that one should not confuse the *volatile* memristive behavior of the present and of Mott devices, with the more commonplace and qualitatively different *non-volatile* type [15, 23, 24]. The latter is used to implement arrays of electronic synapses [25] and resistive random access memories [26].

We now turn to the description of the MSN-IF model of figure 1(e). Under the excitation of a constant current I_{in} the circuit emits a succession the electric spikes, such as the one shown in the top right panel of figure 2. During the spike generation, the voltage-gated conductance $g(V)$ of the M device shows a close periodic orbit, which is shown in the main panel of figure 2. We observe that $g(V)$ commutes between open and closed states (low/high conductance) that essentially correspond to the internal state variable S in equation 2. The commutations low-to-high and high-to-low are indicated by color dots, along the orbit and in the spike-trace (top-right inset), and are also correlated to the respective work-points on the I–V characteristics of the M device (left top-panel). The periodic orbit of $g(V)$ illustrates the history-dependent behavior, which is a feature of the memristive conductance channel. The variation of g along the time-period plays an analogous role to the dynamical equations of the channels in the conventional conductance models.

Upon excitation with a constant current I_{in} the membrane potential V of an ideal IF neuron increases as $V(t) = [I_{in}/C_m]t$, and suddenly discharges with a spike when $V(t) = V_{th}$. Hence, an IF neuron model emits spikes at a frequency $f(I_{in}) = I_{in}/[C_m V_{th}]$, i.e. linear in the applied I_{in}. This behavior is qualitatively well reproduced by our neuron, as seen in the lower left panel of figure 2.

However, there are evident departures from the simple linear behavior at both onsets of excitability, i.e. at the ends of the range $I_{in}^{min} < I_{in} < I_{in}^{max}$. We recall that *excitability* refers to non-linear spiking response of the system to a constant input. In the present model there are two onsets of excitability, denoted I_{in}^{min} and I_{in}^{max}. Within this interval the system shows spiking behavior, otherwise the system is quiescent.

The reason for the departure from the linear behavior at I_{in}^{min} is because the conductance of the M device in the open state is not zero as in an ideal switch, which results a leakage current. Therefore, there is a finite input current that is needed to overcome that leak and excite the spiking. Hence, the neuron model of figure 1(e) may be better characterized as an LIF model. Indeed, we show in the lower left panel of figure 2 that the $f(I_{in})$ is well captured by the expression derived from the LIF model, which demonstrates the type 1 excitability of the MSN [12]. We recall that type 1 excitability refers to a system that starts spiking from zero frequency [2, 12]. The origin of the excitability onset at I_{in}^{max} is different. It follows from the fact that I_{in} is higher that I_{hold}, therefore once the thyristor commutes to the low conductance state, it does not switch back. Hence, instead of spiking behavior, there is a continuous high current across the M device. This high current quiescent state, with $I_{in} > I_{in}^{max}$, is similar to the 'depolarization' state in biological neurons. On the other hand, the low current quiescent state, with $I_{in} < I_{in}^{min}$ is similar to the 'hyper-polarization' state [2].

To complete this introductory discussion it is useful to consider some orders of magnitude to realize that, conveniently, the MSN model produces spiking behavior on timescales compatible with biological neurons. Indeed, since the T has a V_{th} of the order of the volt and a holding current of the order of 100 μA, then adopting a $C_m = 10\,\mu$F we may estimate a spiking frequency $f \sim [100\,\mu\text{A}/(10\,\mu\text{F}\,1\,\text{V})] \sim 10$ Hz. Moreover, the duration of the spike is given by the discharge timescale that we may estimated as $\tau_{spike} \sim C_m/g_{high} \sim [10\,\mu\text{F}/10\,\text{mS}] \sim 1$ ms, similar as in biological neurons. To choose the value of R we consider that the IF behavior requires the leak to be relatively small and also that the charging time-constant $\tau_m \sim RC_m$ must be larger than the inter-spike interval (ISI) $\sim 1/f \sim 0.1$ s. Thus, in our circuit we adopt $R = 100\,\text{k}\Omega$, so $\tau_m \sim RC_m = 1\,\text{s} >>$ ISI. The present circuit is based on the LIF model previously introduced [27–29]. However, the new MSN model achieves further conceptual and practical simplicity, providing a clear basis to build and understand the two-compartment bursting model that we introduce below.

3. The memristive spiking bursting neuron model

We now introduce a novel memristive spiking bursting neuron (MSBN) model of unprecedented simplicity. The model is obtained by equipping the basic MSN circuit figure 1(e) with a second time-constant $\tau_S = R_S C_S$ as shown in figure 3.

In regard of the analogy made before with the conventional conductance models, the voltage of the second capacitor V_S introduces an additional dynamical variable. This increases the dimensionality of the model, which is a necessary condition for the generation of intrinsic bursts [12]. More precisely, this second dynamical variable introduces an additional modulation of the conductance current I_{ion} in equation (2). Thus, the model equations become,

$$C_m \frac{dV}{dt} = I_{ion}(g, \tau_S) + I_{in} \tag{3}$$

$$I_{ion} = g(V, S)(V - V_S) \tag{4}$$

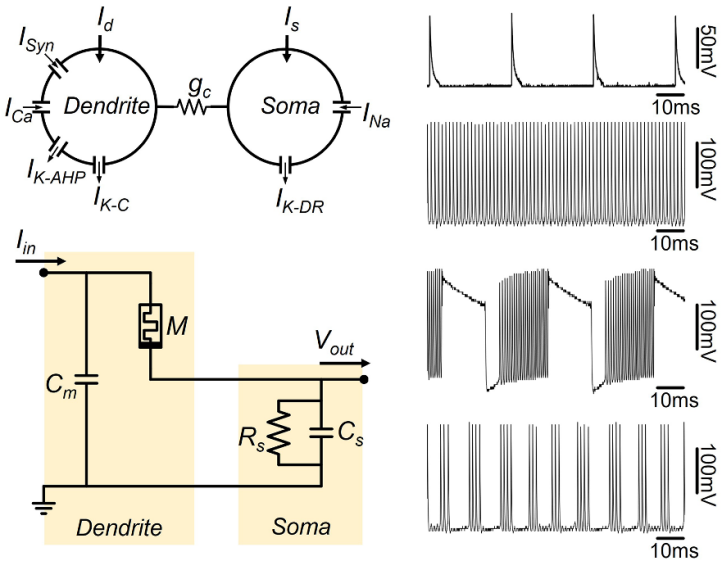

Figure 3. (Top left) Schematic diagram of the Pinsky–Rinzel two-compartment model (bottom left) Schematic of the two-compartment MSBN circuit. (Right) Samples of the different spiking behaviors: tonic spiking (top), fast spiking (second top), intrinsic bursting 1 (bottom), and intrinsic bursting 2 (third from top). Parameter values (C_m and R are the same as in figure 2 above): TS is obtained at (I_{in}, R_s, C_s) = (72.2 μA, 47Ω, 0.1 μF); FS at (46.7 μA, 2.4 kΩ, 0.1 μF); IB2 at (75.1 μA, 2.4 kΩ, 0.1 μF); IB1 at (38.7 μA, 3 kΩ, 0.1 μF).

$$C_S \frac{dV_S}{dt} = I_{ion} - \frac{C_S}{\tau_S} V_S \tag{5}$$

where we observe that the last equation has the same form as the dynamical equation of [Ca]-current in standard theoretical bursting neuron models [12].

However, there is a significant qualitative difference between those mathematical models and the MSBN one. The second time-constant that is introduced in the former models is usually a slow one. Its role is mainly to slowly modulate the tonic spike (TS) generation by driving the neuron in-and-out of its excitability range. In contrast, in the MSBN model the second time-constant τ_S is smaller than the tonic spiking one τ_m, i.e. $\tau_S << \tau_m$. In fact, τ_S is of the same order of the discharge time τ_{spike}, which is also a very small timescale. This feature has two main consequences: firstly, it leads to the emergence of a qualitatively different fast spiking (FS) mode, characterized by a high frequency ($\sim 1/\tau_S$). Secondly, two new additional spiking modes emerge displaying *bursting behavior* (IB1 and IB2). Specifically, IB1 and IB2 appear to be associated to the onsets of excitability of the FS state, at low and high I_{in}, respectively.

It is also worthwhile looking at the MSBN under a different light to appreciate its connection with a well known model of bursting neurons introduced by Pinsky and Rinzel (PR) [31]. It is a two-compartment model, where a dendrite and a soma compartment are coupled by a conductance g_c, as we schematically show in figure 3. This model is a simplified version of an earlier one introduced by Traub *et al* which included 19 conductance channels [32]. These models are aimed at biological realism and can provide detail on the specific role of individual ionic channels in the spike generation. However, this is achieved at the expense of mathematical complexity, which also makes them impractical to use as a basis for building functional neural networks that are numerically tractable.

Interestingly, the MSBN model can also be cast as two-compartment model, where one represents the dendrite and the other the soma (figure 3). In the MSBN the two compartments are directly connected, corresponding to the limit of strong electrotonic coupling (large g_c) in the PR model [31] . Another similarity between the models, interesting in the light of our discussion above, is that the second compartment (the soma) is the one with a smaller time-constant. In contrast to the PR model, the formulation of the MSBN is of extreme simplicity, namely, it is a circuit counting just four electronic components (figure 3). Nevertheless, despite this simplicity the emerging dynamical behavior of the MSBN is complex. We illustrate this point by showing the four distinct types of spiking traces in the right panel of figure 3. Quite remarkably, these variety of dynamical behaviors allows us to qualitatively reproduce the traces recorded in bursting biological neurons, as shown in figure 4. We should also emphasize that the

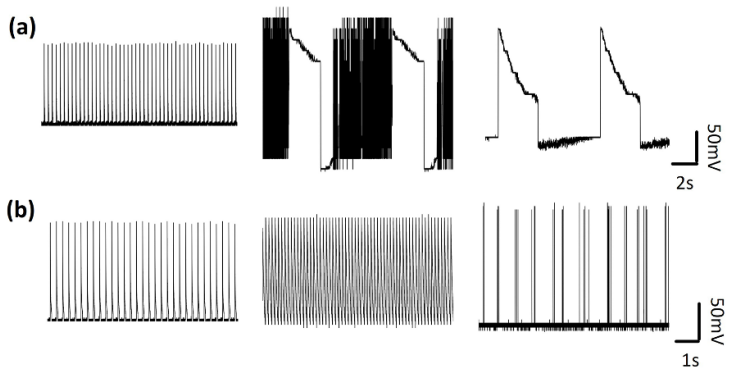

Figure 4. Measured spiking traces of our bursting electronic neuron. We adopted the circuit parameters to qualitatively match the traces (including timescales) obtained in nigral dopamine bursting neuron by Ping and Shepard (see [30] figure 4). The left, middle and right columns of (a) denote TS, IB2, and TS with relatively long discharge time, respectively. The left, middle and right columns of (b) denote TS, FS, and IB1, respectively. Parameter values: TS in (*a*) left is obtained at (C_m, I_{in}, R_s, C_s) = (100 μF, 68.8 μA, 100 Ω, 0.1 μF); IB2 at (2000 μF, 76.2 μA, 2.3 kΩ, 0.1 μF); the wide TS ((*a*) right) at (100 μF, 70.1 μA, 0.9 kΩ, 0.1 μF); TS in (*b*) is obtained at (100 μF, 93.8 μA, 100 Ω, 0.1 μF); FS at (1000 μF, 54.1 μA, 3 kΩ, 33 μF); and IB1 at (1000 μF, 29.4 μA, 6.8 kΩ, 0.47 μF).

comparison between the MSBN traces of figures 3 and 4 demonstrate how easily one can control spiking timescales in the MSBN. In fact, we increased them by two orders of magnitude (from ~10 ms to ~s) to match biological timescales, just increasing the value of the capacitor C_m.

The simplicity of the MSBN circuit can be further exploited to obtain the full phase diagram and explore its global behavior, which provides further insights. In figure 5. we show the four regions of qualitatively distinct spiking behavior, obtained as a function of the input current I_{in} and the soma-compartment time-constant τ_S. For convenience, we fix the capacitor value $C_S = 0.1\,\mu$F so we can scan through τ_S by changing the resistance R_S. We may note that value of C_S is much smaller than the one of the dendrite-compartment ($C_m = 10\,\mu$F). Thus, this choice would correspond to modeling a neuron with a relatively large dendritic tree (i.e. with a large effective area) [33]. Interestingly, all four regions of the phase diagram are relatively large, therefore none of the different spiking behaviors requires of fine tuning to be realized. In the right hand side panels of figure 5. we illustrate some specific instances of spiking traces within each of the four regions.

We may gain further insight from the phase diagram. For instance, we observe that at low τ_S the MSBN shows a region of TS. This is expected, since in this limit both C_S and R_S are relatively small compared to the components of the dendrite compartment. Hence, their effect on the behavior of the system can be considered as a small perturbation with respect to that of the basic MSN, which only produces simple TS.

Interestingly, as τ_S is increased we observe that the TS boundary occurs at a fixed value $\tau_S^* \approx (0.1\,\mu F)(2\,k\Omega) = 0.2$ ms. This independence of the I_{in} value indicates that the termination mechanism is unrelated to the TS frequency. Indeed, the instability of the TS state occurs because the timescale τ_S becomes of the order of the duration of a single spike emission $\tau_{spike} \sim 1$ ms (see figure 2). Hence, when τ_S and τ_{spike} become comparable one can no longer consider the the effect of the former as a small perturbation to simple spiking, and multiple spiking modes emerge.

We describe now the transition from TS to FS states. For the sake of the argument, lets neglect the C_S for the moment. Before the spike emission, the memristor is open, hence its resistance $R_M = 1/g_{low} >> R_S$ and the membrane potential V due to the accumulated charge on C_m mainly falls on M. When V reaches V_{th}, the resistance of the M collapses, and a spike is emitted. However, that sudden change in resistance also implies a sudden change in the voltage division (R_M,R_S). Since now $1/g_{high} << R_S$, only a negligible fraction of V falls on the M. Thus, the M should immediately commute back to the open state (see figure 2) and terminate the spike. However, the V is still at the threshold V_{th}, therefore this paradoxical and seemingly unstable situation indicates that when R_S becomes sufficiently large, the system is no longer able to produce simple spike emission. This instability can be cured by the addition of the small C_S, which brings in a finite time-constant and renders the FS state stable with a high frequency of order $1/\tau_S = 1/(R_S C_S)$. Interestingly, this behavior is qualitatively similar to that of the PR model, where the soma potential is the fast variable that reacts to the excitation of the more slowly varying dendrite [12].

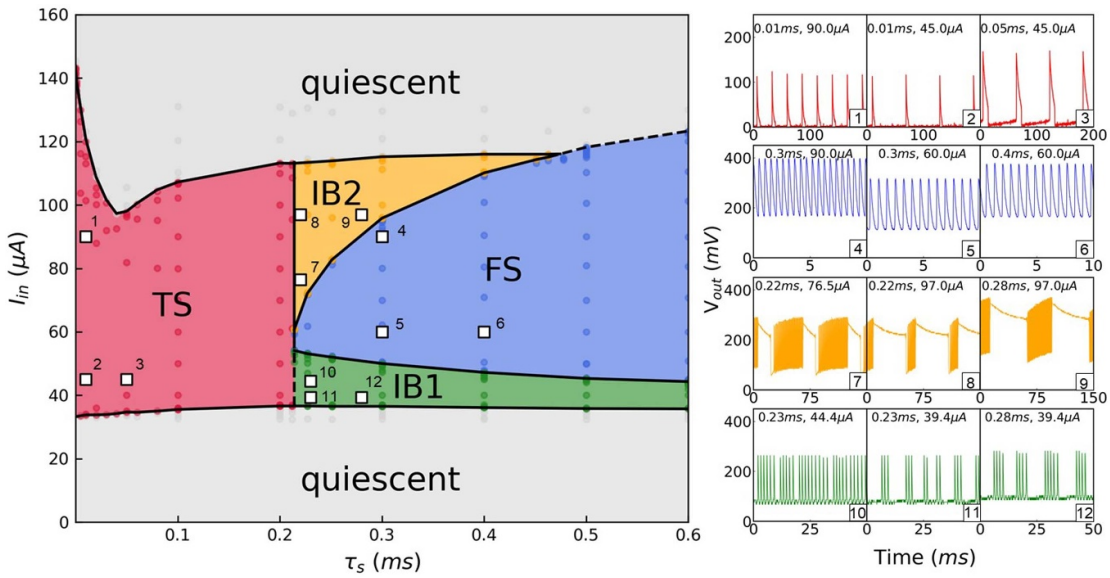

Figure 5. Phase diagram of the bursting circuit obtained as a function of input current $I_{\rm in}$ versus the time-constant of the soma-compartment $\tau_{\rm S}$ (at fixed $C_{\rm s} = 0.1\,\mu$F). TS: tonic spiking (red), FS: fast spiking (blue), IB1: intrinsic bursting 1 (green) and IB2: intrinsic bursting 2 (yellow). On the right side, traces recorded in the phase diagram qualitatively demonstrate the effects on neuronal behavior produced by changing the $I_{\rm in}$ or $\tau_{\rm s}$ respectively. The corresponding positions of all traces in the phase diagram are marked with numbered white squares, and ($\tau_{\rm s}$, $I_{\rm in}$) are indicated in each numbered panel.

We may now qualitatively understand the origin of the intrinsic bursting states, IB1 and IB2. We may note that they both emerge at the two boundaries of excitability, corresponding to the critical currents $I_{\rm in}^{\rm min}$ and $I_{\rm in}^{\rm max}$. As we have seen before in the simpler MSN model case, those boundaries are characterized by the the onset of spiking behavior, which begins with long ISIs. Hence, we may think of each burst as an individual spike-emission event where the spike becomes a short and fast spike-train due to the instability phenomenon described above. The two different line-shapes of the IB1 and IB2 bursts, follow from the fact that they are respectively associated to two qualitatively different onsets of excitability, namely, the hyper-polarized and depolarized states that we discussed before.

4. Navigating the phase diagram and connection to neuroscience

As we emphasized many times already, the salient feature of the MSBN model is its simplicity. A prize to pay is that its parameters are not directly nor obviously connected to biological ones. However, the mapping of the full phase diagram opens an unexpected and exciting perspective. It unveils a global view of the systematic evolution of spiking states, which may provide a new type of guidance in the understanding and interpretation of experiments in neurobiology. More precisely, it may be interesting to search for phenomenological correlations between the systematic behavior of a biological neural system upon changing parameters, such as for instance applying neurotoxins or excitatory currents, and changing the parameters of the circuit-model.

A first example to illustrate this is the above mentioned study of [30] in nigral dopamine neurons, which shows the systematic effects on a regular spiking trace of the successive application of neurotoxins (APA, TTX and TEA). In figure 6(a), we show how the two types of changes in the traces can be respectively located on the phase diagram. In one case, the trace starts from regular tonic spiking, evolves to the IB2-type bursting and then returns back to tonic spiking at a larger $\tau_{\rm s}$ state. In the second case, the trace starts from regular spiking, evolves to FS, and then into IB1-type bursting.

An even more telling example is shown in figure 6(b), where the biological neuron traces (right bottom panel) are reproduced from the study of [34]. There, a pacemaker pre-BötC neuron is first silenced and then subject to a systematically increasing input current. The observation is that the neuron starts to emit bursts with a decreasing inter-burst time interval as the current is increased, until eventually it reaches an FS state. Remarkably, we can qualitatively reproduce the behavior with our model, by solely increasing the applied current (right top panel). This follows a simple vertical path along the phase diagram shown in the left panel.

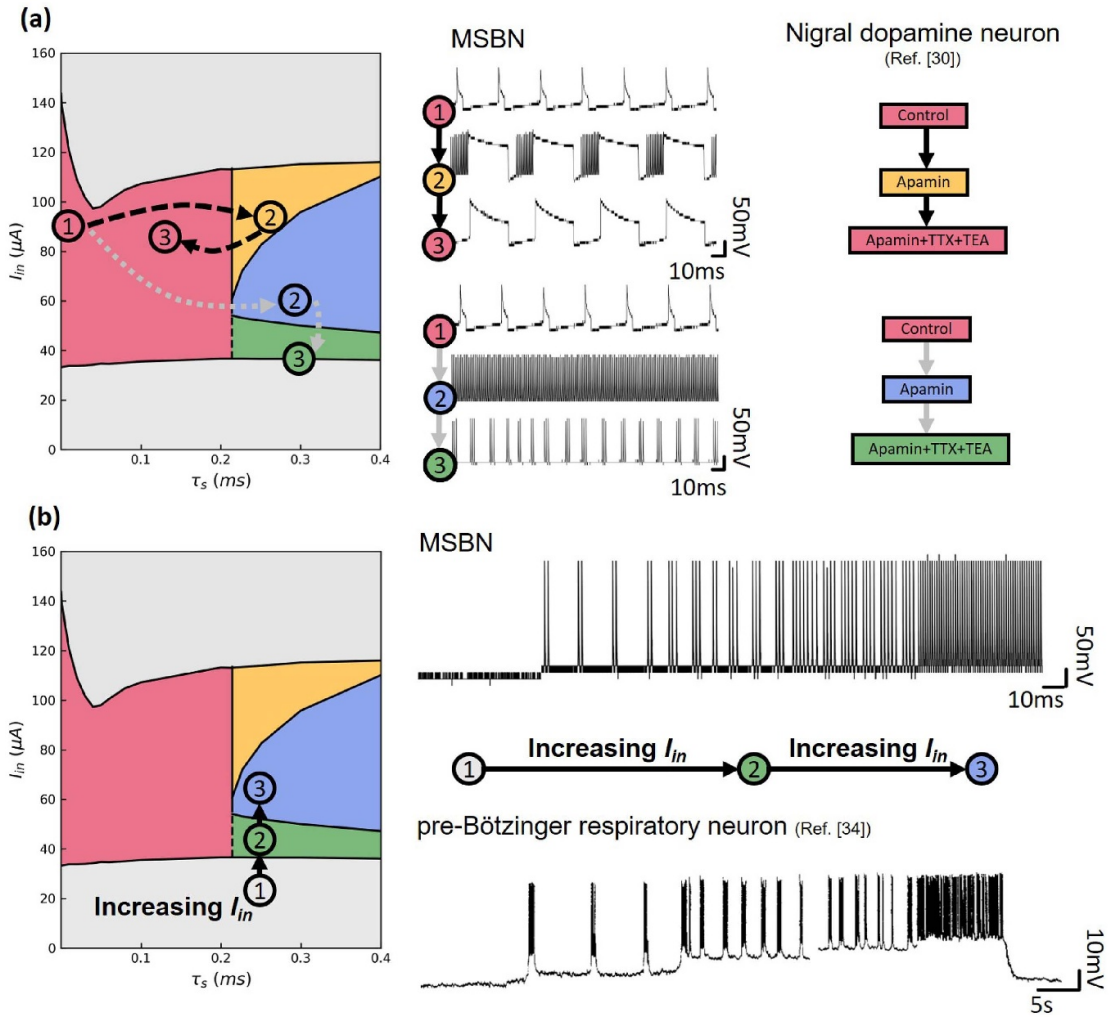

Figure 6. The evolutionary paths in phase diagram can reproduce to some extent the evolution of biological neuronal behavior. (a) The central panel shows the successive spiking states of the MSBN obtained by changing I_{in} and τ_s. The numbers indicate the respective locations, forming a path on the phase diagram, indicated by arrows on the left panel. On the right panel we indicate the 'neurotoxin path' that drives the nigral dopamine neurons to evolve through those spiking states (see figure 4 and [30]). (b) Right panel (top) shows the systematic increase of IB1 bursting to FS by increasing I_{in} in the MSBN. (bottom) A qualitative similar behavior was observed in biological pre-Bötzinger respiratory neurons by increasing the input excitatory current [34]. As in panel (a), the numbers indicate the path along the phase diagram of the MSBN. The parameter pair (I_{in}, R_s) for each of the shown traces are: for panel (a), red-1 trace (89.6 μA, 47 Ω), yellow-2 trace (89.6 μA, 2.6 kΩ), red-3 trace (82.8 μA, 1.3 kΩ), blue-2 trace (58.8 μA, 3.0 kΩ), and green-3 trace (36.5 μA, 3.0 kΩ); for panel (b), R_s is fixed at 2.5 kΩ, and I_{in} are increased from 26.0 μA, to 36.4 μA, 40.8 μA, 46.5 μA, until 52.6 μA. Reproduced with permission from [34]. [© 1999 The American Physiological Society].

As the current increased from 26.0 μA to 52.6 μA, the MSBN changed from a silence state to a bursting state and gradually decreased the inter-burst time interval, eventually changing to an FS state, just as the pacemaker pre-BötC neuron exhibited.

As shown on the left panels, the evolutions of the traces follow paths in the phase diagram, crossing boundaries from one region to another. Hence, we may speculate that this type of observations may one day open the way to provide a rationale and perhaps suggest strategies to treat neural diseases associated to abnormal burst spiking.

5. Conclusions

In this work we have introduced a minimal model for an intrinsic bursting neuron, which is defined by its hardware implementation. The model is of unprecedented simplicity, counting just four components, two capacitors, one resistor and a memristor device.

The MSBN circuit, nevertheless, sustains four types of complex spiking behavior, all of them at relevant biological time-scales and showing wave-forms of striking realism. We have illustrated this feature by comparing spiking traces generated by the MSBN with traces measured in biological neurons.

Implementing and understanding intrinsic bursting mechanisms in simple neuron models is also important from a broader perspective. In fact, bursting neurons are ubiquitous in animals and humans as they are associated to motor behavior. A burst signal is more reliable to command a muscle than a single spike [35, 36]. Well studied examples are the pre-Bötzinger respiratory neurons [34] and the lobster's stomatogastric ganglion [37]. Moreover, understanding the neuronal spike bursting phenomenon is also relevant in regard to neural dysfunctions, such as in Parkinson's disease, epilepsy, depression and forms of autism [38–42].

Several exciting perspectives are also open by our hardware model, which is easy to implement, understand and control; has all out-of-the-shelf components that are readily and cheaply available; and has low-power requirements if compared with CPU-based implementations. We can make an order of magnitude estimate: the energy per spike can be very roughly (and likely over) estimated as CV^2, i.e. $\sim(1\,\mu\text{F})(1\,\text{V})^2 \sim 1\,\mu\text{J}$, or ~0.3 nWh. A conventional button cell battery can deliver a total energy of ~0.3 Wh, which is nine orders of magnitude larger. Hence, this would allow the MSN to spike 10^9 times, i.e. operating at 1 Hz it would last for about 30 years. Hence, it may be an excellent physical platform to develop neuroprostetics, such as neuronal implants for deep brain stimulation in the treatment of Parkinson's disease [43], or low-cost smart pacemakers. Another exciting possibility would be to build brain–machine-interfaces, implementing functional neural networks interfaced via optogenetics in closed-loop systems with essentially zero-delay neuro-computation time.

6. Methods

The electrical characterization of the electronic neurons are performed on the prototypes implemented on breadboard with out-of-the-shelf components.

The I–V curve of the M device (figure 2) is measured in a simple series circuit shown in figure 7(a), where a loading resistor $R_{\text{load}} = 1\,\text{k}\Omega$ is in series with the M device. The voltage drops of the M device (V_0) and the R_{load} (V_1) are measured by an oscilloscope. Then the I–V curve are plotted from V_1/R_{load} vs V_0. The other characteristics of the MSN (figure 2.) are measured in the circuit shown in figure 7(b). In order to finely tuning the input current I_{in}, a standard gate-controlled current mirror with two P-MOS transistors and one N-MOS transistor is applied. The input current of the neuron is measured by an ammeter A. The voltage drop V_0 of the M device and the output signals V_1 (voltage drop on a loading resistor $R_{\text{load}} = 47\,\Omega$) are measured by an oscilloscope. As for the MSBN (figures 3–5), the measurements are carried out on a circuit shown in figure 7(c). To control the input current, the same current mirror part is used. The input current is measured by an ammeter A and the output signals V_1 are collected on the 'soma' part by an oscilloscope.

All the electronic components and instruments used are easy to access. The thyristors used are from STMicroelectonics (P0118MA 2AL3). The current mirror are implemented on dual N-channel and dual P-channel matched MOSFET pair from advanced linear devices (ALD1105). The power sources V_{supply} and V_{control} used for the current mirror are RS Pro RS-3005P and RSDG805 respectively. The multimeter is a Mastech MS8217 and the oscilloscope is a PicoScope 2204A.

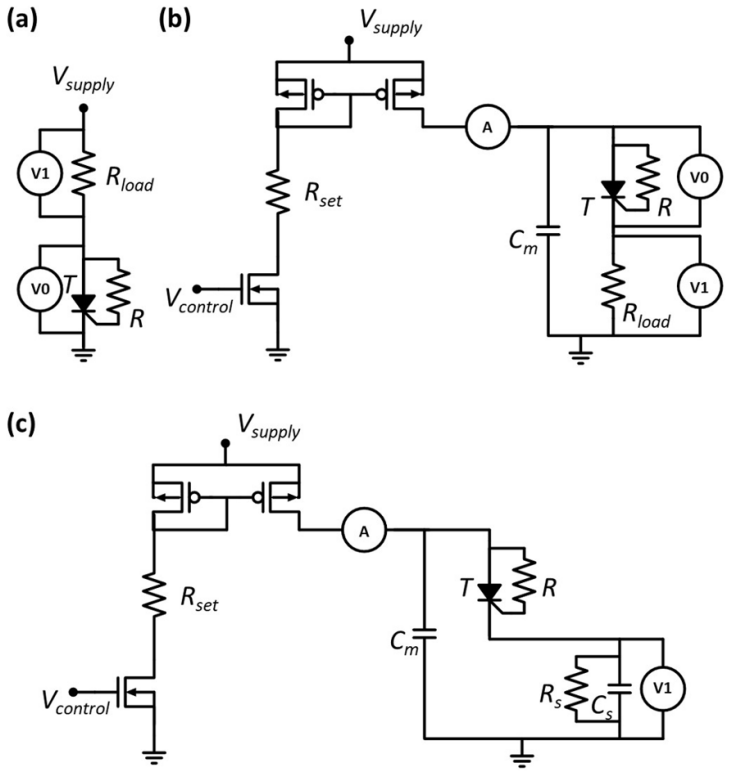

Figure 7. The circuits of the measurements. (a) for *I*–*V* curve measurement; (b) for simple spiking neuron MSN measurement; (c) for bursting neuron MSBN measurement.

Data availability statement

The data cannot be made publicly available upon publication because they are not available in a format that is sufficiently accessible or reusable by other researchers. The data that support the findings of this study are available upon reasonable request from the authors.

Acknowledgments

We acknowledge support from the French ANR 'MoMA' project ANR-19-CE30-0020. We thank C Pasquier and P Senzier for providing space and help to set up of our research activity. This work was initiated within the framework of the AIST-CNRS-CentraleSupélec Joint Research Agreement 'Bioinspired electronic systems'.

ORCID iD

Marcelo Rozenberg https://orcid.org/0000-0001-9161-0370

References

[1] Herz A V M, Gollisch T, Machens C K and Jaeger D 2006 Modeling single-neuron dynamics and computations: a balance of detail and abstraction *Science* **314** 80
[2] Gerstner W, Kistler W, Naud R and Paninski L 2014 *Neuronal Dynamics: From Single Neurons to Networks and Models of Cognition* (Cambridge University Press)
[3] Hopfield J J 1982 Neural networks and physical systems with emergent collective computational abilities *Proc. Natl Acad. Sci.* **79** 2554
[4] Hodgkin A L and Huxley A F 1952 A quantitative description of membrane current and its application to conduction and excitation in nerve *J. Physiol.* **117** 500
[5] Merolla P A, Arthur J V, Alvarez-Icaza R, Cassidy A S, Sawada J, Akopyan F, Jackson B L, Imam N, Guo C and Nakamura Y 2014 A million spiking-neuron integrated circuit with a scalable communication network and interface *Science* **345** 668
[6] Thakur C S *et al* 2018 Large-scale neuromorphic spiking array processors: a quest to mimic the brain *Front. Neurosci.* **12** 891
[7] Stoliar P, Tranchant J, Corraze B, Janod E, Besland M-P, Tesler F, Rozenberg M and Cario L 2017 A leaky-integrate-and-fire neuron analog realized with a mott insulator *Adv. Funct. Mater.* **27** 1604740
[8] Pickett M D, Medeiros-Ribeiro G and Williams R S 2013 A scalable neuristor built with Mott memristors *Nat. Mater.* **12** 114

[9] Yi W, Tsang K K, Lam S K, Bai X, Crowell J A and Flores E A 2018 Biological plausibility and stochasticity in scalable VO_2 active memristor neurons *Nat. Commun.* **9** 4661
[10] Rocco R, del Valle J, Navarro H, Salev P, Schuller I K and Rozenberg M 2022 Exponential escape rate of filamentary incubation in mott spiking neurons *Phys. Rev. Appl.* **17** 024028
[11] Izhikevich E M 2000 Neural excitability, spiking and bursting *Int. J. Bifurcat. Chaos* **10** 1171
[12] Ermentrout G and Terman D 2010 *Mathematical Foundations of Neuroscience, Interdisciplinary Applied Mathematics* (Springer)
[13] Leon Chua V S and Kim H-S 2012 Hodgkin–Huxley axon is made of memristors *Int. J. Bifurcat. Chaos* **22** 1230011
[14] Chua L 2014 If it's pinched it's a memristor *Semicond. Sci. Technol.* **29** 104001
[15] del Valle J, Ramírez J G, Rozenberg M J and Schuller I K 2018 Challenges in materials and devices for resistive-switching-based neuromorphic computing *J. Appl. Phys.* **124** 211101
[16] Wang R, Yang J-Q, Mao J-Y, Wang Z-P, Wu S, Zhou M, Chen T, Zhou Y and Han S-T 2020 Recent advances of volatile memristors: devices, mechanisms and applications *Adv. Intell. Syst.* **2** 2000055
[17] Yang K, Joshua Yang J, Huang R and Yang Y 2022 Nonlinearity in memristors for neuromorphic dynamic systems *Small Sci.* **2** 2100049
[18] Hoffmann A *et al* 2022 Quantum materials for energy-efficient neuromorphic computing: opportunities and challenges *APL Mater.* **10** 070904
[19] Wang Y-H, Gong T-C, Ding Y-X, Li Y, Wang W, Chen Z-A, Du N, Covi E, Farronato M and Ielmini D 2022 Redox memristors with volatile threshold switching behavior for neuromorphic computing *J. Electron. Sci. Technol.* **20** 100177
[20] Stoliar P, Cario L, Janod E, Corraze B, Guillot-Deudon C, Salmon-Bourmand S, Guiot V, Tranchant J and Rozenberg M 2013 Universal electric-field-driven resistive transition in narrow-gap Mott insulators *Adv. Mater.* **25** 3222
[21] Del Valle J, Salev P, Tesler F, Vargas N M, Kalcheim Y, Wang P, Trastoy J, Lee M-H, Kassabian G and Ramírez J G 2019 Subthreshold firing in Mott nanodevices *Nature* **569** 388
[22] Sze S M and Ng K K 2006 *Physics of Semiconductor Devices* 3rd edn (Wiley-Interscience)
[23] Covi E, Wang W, Lin Y-H, Farronato M, Ambrosi E and Ielmini D 2021 Switching dynamics of Ag-based filamentary volatile resistive switching devices-part I: experimental characterization *IEEE Trans. Electron Devices* **68** 4335
[24] Zhou G, Wang Z, Sun B, Zhou F, Sun L, Zhao H, Hu X, Peng X, Yan J and Wang H *et al* 2022 Volatile and nonvolatile memristive devices for neuromorphic computing *Adv. Electron. Mater.* **8** 2101127
[25] Kim H, Mahmoodi M R, Nili H and Strukov D B 2021 4k-memristor analog-grade passive crossbar circuit *Nat. Commun.* **12** 5198
[26] Zahoor F, Azni Zulkifli T Z and Khanday F A 2020 Resistive random access memory (RRAM): an overview of materials, switching mechanism, performance, multilevel cell (mlc) storage, modeling and applications *Nanoscale Res. Lett.* **15** 90
[27] Rozenberg M J, Schneegans O and Stoliar P 2019 An ultra-compact leaky-integrate-and-fire model for building spiking neural networks *Sci. Rep.* **9** 11123
[28] Stoliar P, Schneegans O and Rozenberg M J 2020 Biologically relevant dynamical behaviors realized in an ultra-compact neuron model *Front. Neurosci.* **14** 421
[29] Stoliar P, Schneegans O and Rozenberg M J 2021 A functional spiking neural network of ultra compact neurons *Front. Neurosci.* **15** 635098
[30] Ping H and Shepard P 1996 Apamin-sensitive Ca (2+)-activated K+ channels regulate pacemaker activity in nigral dopamine neurons *Neuroreport* **7** 809
[31] Pinsky P F and Rinzel J 1994 Intrinsic and network rhythmogenesis in a reduced traub model for CA3 neurons *J. Comput. Neurosci.* **1** 39
[32] Traub R D, Wong R K, Miles R and Michelson H 1991 A model of a CA3 hippocampal pyramidal neuron incorporating voltage-clamp data on intrinsic conductances *J. Neurophysiol.* **66** 635
[33] Connors B W and Regehr W G 1996 Neuronal firing: does function follow form? *Curr. Biol.* **6** 1560
[34] Butera Jr R J, Rinzel J and Smith J C 1999 Models of respiratory rhythm generation in the pre-Bötzinger complex. I. Bursting pacemaker neurons *J. Neurophysiol.* **82** 382
[35] Kepecs A and Lisman J 2003 Information encoding and computation with spikes and bursts *Netw. Comput. Neural Syst.* **14** 103
[36] Zeldenrust F, Wadman W J and Englitz B 2018 Neural coding with bursts—current state and future perspectives *Front. Comput. Neurosci.* **12**
[37] Russell D F and Hartline D K 1978 Bursting neural networks: a reexamination *Science* **200** 453
[38] Beurrier C, Congar P, Bioulac B and Hammond C 1999 Subthalamic nucleus neurons switch from single-spike activity to burst-firing mode *J. Neurosci.* **19** 599
[39] Prince D A and Wong R K 1981 Human epileptic neurons studied in vitro *Brain Res.* **210** 323
[40] Yang Y, Cui Y, Sang K, Dong Y, Ni Z, Ma S and Hu H 2018 Ketamine blocks bursting in the lateral habenula to rapidly relieve depression *Nature* **554** 317
[41] Lee E *et al* 2021 Excitatory synapses and gap junctions cooperate to improve Pv neuronal burst firing and cortical social cognition in Shank2-mutant mice *Nat. Commun.* **12** 5116
[42] Das Sharma S *et al* 2020 Cortical neurons derived from human pluripotent stem cells lacking FMRP display altered spontaneous firing patterns *Mol. Autism* **11**
[43] Rubin J E and Terman D 2004 High frequency stimulation of the subthalamic nucleus eliminates pathological thalamic rhythmicity in a computational model *J. Comput. Neurosci.* **16** 211